

# Journal of Materials Chemistry C

Accepted Manuscript



This is an *Accepted Manuscript*, which has been through the Royal Society of Chemistry peer review process and has been accepted for publication.

*Accepted Manuscripts* are published online shortly after acceptance, before technical editing, formatting and proof reading. Using this free service, authors can make their results available to the community, in citable form, before we publish the edited article. We will replace this *Accepted Manuscript* with the edited and formatted *Advance Article* as soon as it is available.

You can find more information about *Accepted Manuscripts* in the [Information for Authors](#).

Please note that technical editing may introduce minor changes to the text and/or graphics, which may alter content. The journal's standard [Terms & Conditions](#) and the [Ethical guidelines](#) still apply. In no event shall the Royal Society of Chemistry be held responsible for any errors or omissions in this *Accepted Manuscript* or any consequences arising from the use of any information it contains.

# Extremely Flexible, Printable Ag Conductive Features on PET and Paper Substrate *via* Continuous Milisecond Photonic Sintering in a Large Area

Cite this: DOI: 10.1039/x0xx00000x

Received 00th January 2012,  
Accepted 00th January 2012

DOI: 10.1039/x0xx00000x

www.rsc.org/

Yejin Jo,<sup>a</sup> Sang-Jin Oh,<sup>a</sup> Sun Sook Lee,<sup>a</sup> Yeong-Hui Seo,<sup>a</sup> Beyong-Hwan Ryu,<sup>a</sup>  
Jooho Moon,<sup>b</sup> Youngmin Choi,<sup>a,\*</sup> Sunho Jeong<sup>a,\*</sup>

The development of highly conductive, flexible metallic constituents in patterned geometries has been of paramount interest in various optoelectronic applications. Among a variety of materials, silver nanoparticles have been considered a candidate that meets the physical/chemical requirements for practical applications; but, the issues for applicability to roll-to-roll processes on inexpensive substrates have not been still resolved. In this study, we demonstrate that the highly flexible, rollable, printable Ag structures, with an electrical resistivity of 8.0  $\mu\Omega\cdot\text{cm}$ , are easily formed in a timescale of  $10^{-3}\text{sec}$  on polyethylene terephthalate and paper substrates, by supplying the highly intensive photon energies on olate-Ag nanoparticle assemblies. The precise control on the amount of carbon residues, by a virtue of sophisticatedly adjustable input of photon energies, allow for the formation of well-adhesive metallic films on plastic substrates, without incorporating any additional procedures, enabling for the extreme flexibility during 10,000 cycles at a bending radius of 1.5 mm. The continuous approach with a moving stage also suggests the potential toward a practical sintering process for instantly generating the highly flexible, conductive metallic architectures in a large area.

## 1. Introduction

In recent decades, the development of liquid-phase, highly conductive metal nanoparticles has attracted tremendous attention, and enabled a variety of applications in the field of flexible optoelectronics, such as radio frequency identifications, solar cells, displays, thin-film transistors, and printed circuit boards.<sup>1-4</sup> In particular, metal printing technologies, unlike time-consuming, complex photolithography methods, offer the fundamental possibility of disposable and large-area flexible applications at greatly reduced costs. Printable metal nanoparticles need to meet various requisites, including high conductivity, chemical/environmental stability, printability, and processability on inexpensive polyethylene terephthalate (PET)/paper substrates. Moreover, most importantly, for use with high-throughput roll-to-roll (R2R) based printing technologies, they require an effective sintering process, which is essential to forming conductive pathways by microstructural densification. To be practical, this process should be completed in a very short time over a large area.<sup>5</sup>

To address those issues, size-controlled nanometer scale Ag particles have been recently researched with a photonic sintering process that uses the instant irradiation of highly intensive photons.<sup>5-10</sup> For conventional thermal annealing processes, thermal energy must be supplied for a prolonged time, longer than at least 10 min, to trigger sufficient mass

transport between neighboring nanoparticles.<sup>11-14</sup> In R2R processes, the heat-treatment zone is applied to a rapidly moving carrier film stage, which requires the thermal zone to be extremely long in order to produce an annealing effect of more than 10 min. In contrast, the photonic sintering process facilitates an instant, vigorous microstructural evolution from particulate assemblies to conductive, dense metal frameworks. Other methodologies such as plasma-,<sup>15-18</sup> laser-,<sup>19</sup> and microwave-based<sup>20,21</sup> sintering can also be used to rapidly generate the conductive features without adverse effects on underlying substrates. But compared with the photonic sintering methodology, which employs a relatively cheap, easily scalable light source, those processes either involve significant costs in preparing the apparatus that generates the reactive chemical/photonic energy, or practical difficulties in scaling up for large-area applications. Recently, a sequential printing-based chemical sintering process has opened up the new possibility of room-temperature processable metal nanoparticle assemblies.<sup>22-24</sup> However, this approach requires a specific chemical pair-reaction between capping molecules anchored to nanoparticle surfaces and additionally incorporated chemical agents.

To date, the instant generation of highly conductive printed Ag structures via the photonic sintering technique has not been demonstrated to produce acceptable flexibility with repeated bending tests on economically desirable substrates, such as

polyethylene terephthalate (PET), because the vulnerable polymeric PET substrate is degraded during the intensive photonic sintering process. Resistivity of  $\sim 150 \mu\Omega\text{-cm}$  has been reported for PET substrates,<sup>8</sup> while the lowest resistivity, comparable to that of bulk Ag, has been obtained on glass, polyimide (PI), poly(ethylene naphthalate), and composite substrates.<sup>5-10</sup> The successful use of Cu nanoparticles for instantly sintered Cu conductive structures with bulk-like electrical conductivities has not yet been reported.<sup>25,26</sup> This is partly because producing Cu nanoparticles without surface oxidation is quite challenging, due to the thermodynamic stability of oxide phases. The resulting higher melting point and the inefficient mass transport through surface oxide layers requires higher energy input to induce a morphological evolution toward conductive bulk structures.<sup>27</sup>

In this study, we demonstrate highly conductive, flexible Ag features generated on both PET and paper substrates by using a well-optimized photonic sintering process with wet-chemically synthesized olate-Ag nanoparticles, without photochemical damage on underlying substrates. The controlled supply of photon energies in a timescale of  $\sim$ msec produces adhesive film properties on plastic substrates without the use of organic/inorganic adhesive promoters, showing extremely good flexible characteristics during 10,000 cycle repeated bending tests under a bending radius of 1.5 mm. Combining the continuous photonic sintering with a moving stage shows the method's practical potential for application in large-area R2R processes.

## 2. Experimental

Octylamine ( $\text{C}_8\text{H}_{17}\text{NH}_2$ , 99%), oleic acid ( $\text{C}_{18}\text{H}_{34}\text{O}_2$ , 90%), phenylhydrazine ( $\text{C}_6\text{H}_5\text{NHNH}_2$ , 97%) and toluene ( $\text{C}_6\text{H}_5\text{CH}_3$ , anhydrous, 99.8%) were purchased from Sigma Aldrich, and Ag nitrate ( $\text{AgNO}_3$ , 99.9%) was purchased from Kojima Chemicals. For synthesizing Ag nanoparticles, 9.5 g of Ag nitrate and 25.4 ml of oleic acid were added into a three-neck round-bottomed flask containing 93.2 ml of octylamine. The prepared reacting solution was heated to 80 °C and stirred with magnetic stirrer under a refluxing condition. When the temperature approached 80 °C, 87.4g of phenylhydrazine was injected with an injection rate of 5 ml/min. The reaction was continued for 60 min and then cooled to room temperature. The synthesized Ag nanoparticles were washed with toluene by centrifugation. For preparation of the Ag conductive ink with a solid loading of 20 wt%, synthesized Ag nanoparticles were dispersed with a dispersant, a high molecular weight block copolymer with an amine number of 10 mg KOH/g, in toluene. Then, the prepared ink was processed by ball milling for 1 hr in order to break soft agglomerates, followed by a drop casting on PI (PNSS, 75  $\mu\text{m}$ ), PET (Dupont, 125  $\mu\text{m}$ ) and photo paper (Epson ultra premium photo paper glossy, 297  $\text{g}/\text{m}^2$ ) substrate. The cast Ag films were dried at room temperature for 10 min. For pen printing, the Jeller pen (Monami Co., Ltd.) was used in this study. The ink barrel was separated from the rollerball tip and cleaned with ethanol. Then, the prepared Ag conductive ink was loaded into the ink barrel. The pen printing was performed by hand on each substrate, followed by drying at room temperature for 10 min.

For transforming the Ag particulate films into conductive layers, the films were thermally treated by conventional annealing on a hot plate at 100, 150, 200, 250, and 300 °C for 1 h. The ramping rate was 5 °C/min. Photonic annealing was accomplished using a xenon flash lamp system (Sinteron 2010,

Xenon Corp.) in which the B type lamp was equipped with a broadband spectrum of 240 to 800 nm. The flash lamp dimension was 0.8 cm in width and 40 cm in length, and the size of the moving stage was 900  $\text{cm}^2$ . The air cooled xenon linear flash lamp, located 2 inch away from a substrate stage, delivered optical energy of from 0.39 to 2.44  $\text{J}/\text{cm}^2$ , as a function of an electrical voltage and a duration time, for generating the electrical pulse energies. The optical energies of the flash lamp irradiation were measured by radiometer (ITL1700, International Light Technologies) with detector (SED033, 200-1100 nm, International Light Technologies), and the substrate temperatures during photo-annealing were detected with a thermometer (1311A, K-Type, TES) and thermo-indicator (3MC-40/55/70, AS TOOL).

The size and shape of the synthesized Ag nanoparticles, and the microstructures of Ag conductive layers were examined by transmission electron microscopy (TEM, JEM-4010, JEOL) and scanning electron microscopy (SEM, JSM-6700, JEOL), respectively. The crystal structure of the Ag nanoparticles was analyzed using an X-ray diffractometer (XRD, D/MAX-2200V, Rigaku), and chemical structural analysis of the Ag nanoparticles/layers was performed with X-ray photoelectron spectroscopy (XPS, K-Alpha, Thermo Fisher Scientific). The absorption spectra for the Ag nanoparticle ink was measured using a UV-Vis spectroscopy (UV-2501PC, 200-1100 nm, Shimadzu). The thermal behavior of the Ag nanoparticles was monitored using thermal gravimetric analysis (SDT2960, TA Instruments) with a heating rate of 5 °C/min. The resistivity of Ag conductive layers was analyzed by a four point probe (FPP-HS8, Dasol Eng.) with a bending machine (PMC-1HS, Autonics). For measuring the variation of resistivity with repeated bending tests, the drop-casted, photo-sintered (at 2.0 kV for 1.5 msec for PET substrates, and at 3.0 kV for 1.0 msec for PI substrates) Ag films on polymer substrates were loaded in the bending machine. The resistivities of samples were measured in a flat state after completing the specific number of cycles, and the average resistivity data were obtained from 5 different samples. The adhesion tests were carried out with a tape, used in ASTM 3359. The tape was attached on top of photo-sintered Ag films, and the surface of tape was rubbed for forming a firm contact. Then, the tape was detached gently from the Ag films.

## 3. Results and Discussion

Ag nanoparticles were synthesized through the chemical reduction of Ag ions, derived from Ag nitrates, in octylamine, a solvent medium, incorporating oleic acid. Oleic acid acted as a surface capping agent to prevent undesirable inter-particle aggregation during the vigorous chemical reaction, as well as endowing the dispersion stability by establishing a long linear chain structure. After completion of the synthetic reaction, Ag nanoparticles, obtained after a repeated washing procedure, were readily dispersed in non-coordinating solvents such as toluene and benzene. The resulting Ag nanoparticles appeared to be individually separated without the formation of agglomerated particle assemblies, with a spherical morphology and a diameter below 10 nm (Figure 1a). Both X-ray diffraction and X-ray photoelectron spectroscopy results revealed that the Ag nanoparticles were phase-pure, not accompanied by the formation of any other secondary phases (Figure 1b and c). The well-separated morphology, diameter of a few tens of nanometers, and the phase purity of the crystalline structures are critical to the thermal or optical energy-induced structural

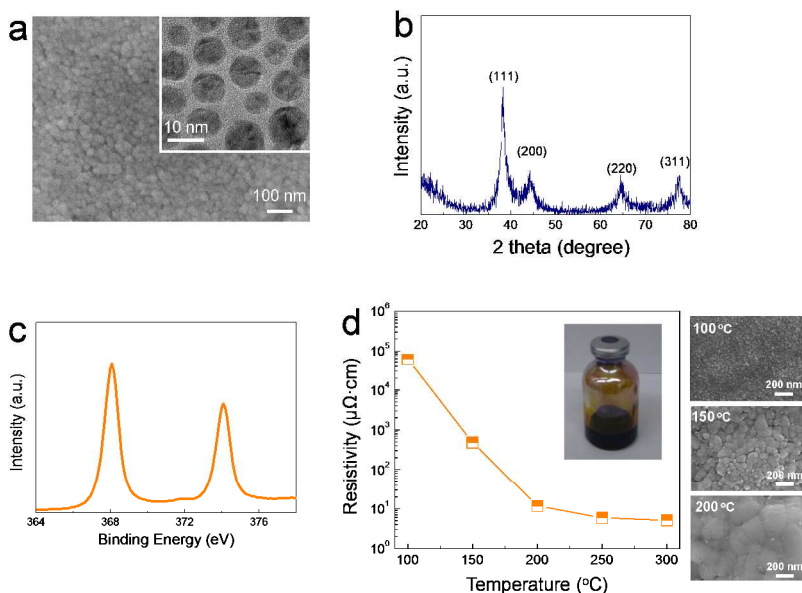


Figure 1. (a) Scanning electron microscopy image, (b) X-ray diffraction result, and (c) Ag 3d X-ray photoelectron spectroscopy spectrum for synthesized Ag nanoparticles. The two peaks in the XPS spectrum are located at 368.1 and 374.1 eV, corresponding to Ag 3d<sub>5/2</sub> and 3d<sub>3/2</sub> binding energy, respectively, without any other peaks including oxide phases present at lower binding energies. (d) Resistivity variation and SEM images of Ag particulate films annealed at different temperatures for 60 min. Inset is a photograph of prepared Ag nano-ink.

transformation of particulate films into conductive bulk structures. The melting point of metal nanoparticles is drastically lowered to extremely low temperatures, even comparable to plastic substrates, as a function of the nanoparticle diameter. The impure phases interrupt the structural transformation in metallic particulate films when external energy is applied to trigger the mass transport.<sup>11-14</sup> As shown in Figure 1d, the Ag particulate films started undergoing a temperature-dependent structural evolution after annealing at 150 °C for 60 min. After annealing was completed above 250 °C, the films showed a bulk-like resistivity of 5.8 μΩ·cm. The resistivity of pure bulk Ag is 1.6 μΩ·cm. Considering the inherent high melting point for Ag phase, 1234 °C, this low temperature processability and resulting low electrical resistivity was achievable because of the aforementioned nanoparticle's well-designed morphological and crystalline properties. However, an annealing temperature above 200 °C is still not acceptable for practical large-area, flexible applications based on cost-effective PET and paper substrates.

The photo-sintering methodology suggested in this study uses a highly intensive light ranging from 240 to 800 nm. The instant supply of photon energy allows Ag nanoparticle-based films to be converted into highly conductive layers in a timeframe of ~ msec. The Ag nanoparticles effectively absorb the UV-visible light, with plasmonic resonance characteristics (Figure 2). Figure 3 shows the resistivity evolution for Ag nanoparticle films prepared on plastic substrates, depending on photon generating conditions, voltage and time. The dose of photon energy was controlled as a function of electrical voltage and duration time, as shown in Figure S1. The energy dose was adjusted in the range of 0.39 - 3.44 J/cm<sup>2</sup> depending on photon generating conditions, and the intensity was linearly controlled from 847 to 1,759 W/cm<sup>2</sup> by increasing the voltage. The linear incremental trend of intensity as a function of voltage is

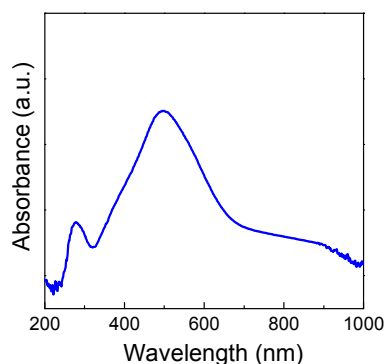


Figure 2. UV-Visible spectroscopy result for Ag nanoparticle film on a glass substrate. The absorption background by the glass substrate was subtracted.

indicative of the accuracy in measuring photon energies irradiated for ~ msec.

To elucidate the photo-annealing effect without concern for substrate deformations, a polyimide substrate was used prior to the tests with PET and paper substrates (Figure 3a). Below 1.5 kV, the Ag nanoparticle film was still resistive regardless of duration times. When photon energy was generated at 2.0 kV for a time longer than 1.5 msec, a resistivity of 7 - 8 μΩ·cm was measured for instantly treated Ag nanoparticle films. At 2.5 - 3.0 kV, highly conductive films were obtained even after a shorter duration time of 1.0 msec. The photo-annealing at 3.0 kV with a duration time longer than 1.5 msec resulted in the partial delamination of Ag films from substrates, owing to the overdose of photon energy. The absorption of photons in Ag particulate films and its contribution to structural transformations were confirmed by the variation of substrate temperatures between bare substrates and Ag nanoparticle

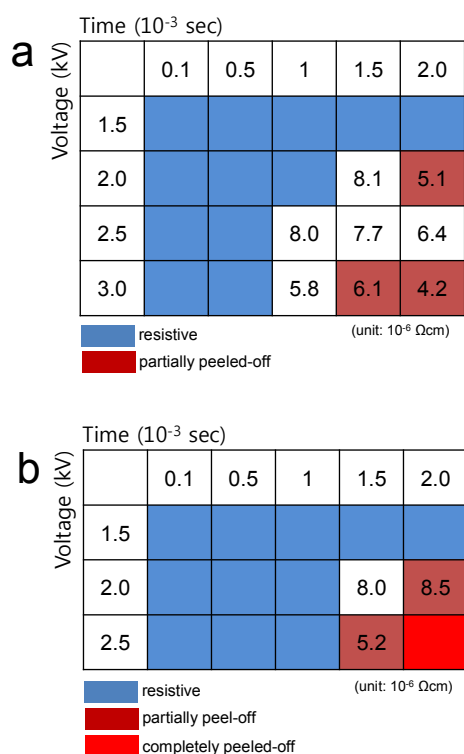


Figure 3. The resistivity evolution of Ag nanoparticle films prepared on (a) PI and (b) PET substrates, after photo-sintering under different conditions.

coated substrates during photon irradiation (Figure S2). Notably, in all photon generating conditions, the substrate temperatures did not exceed  $120\text{ }^{\circ}\text{C}$ , due to the spatial loss of thermal energies which were not absorbed in the Ag layer. The measurement of substrate temperatures was carried out with a thermocouple attached to the backside of the substrates to exclude the effect of heating of the thermocouple itself; however, because of the time delay in detecting substrate temperatures, the temperature could be underestimated to some extent.<sup>28</sup> To further clarify it, we also measured substrate temperatures using thermo-indicators, and the discrepancy between both measurements was not over  $15\text{ }^{\circ}\text{C}$ .

The processability on PET substrates is further evidence that the substrate temperature was maintained below  $150\text{ }^{\circ}\text{C}$  during the photo-sintering process. On PET substrates, a similar trend in resistivity evolutions was observed on PI substrates; when both the electrical voltage and the duration time was increased, the electrically insulating Ag nanoparticle films were converted into highly conductive ones (Figure 3b). The processing parameter window was narrower in this case, due to the more vulnerable physical properties of the PET substrate. Resistivity of  $8.0\text{ }\mu\Omega\text{-cm}$  was obtained after photo-annealing at  $2.0\text{ kV}$  for  $1.5\text{ msec}$ . The slight increment in resistivity with respect to the bulk counterpart is commonly observable for nanoparticle derived conductive films, owing to the subtle presence of organic residues inside the films and the presence of nano- and/or micro-voids.<sup>4,24</sup> These results suggest that instant irradiation with intensive photon energy facilitates the facile generation of highly conductive metallic layers in nanoparticle films prepared from well-formulated Ag nanoparticle colloids, even on thermally vulnerable PET substrates. Notably, this was accomplished without the need to

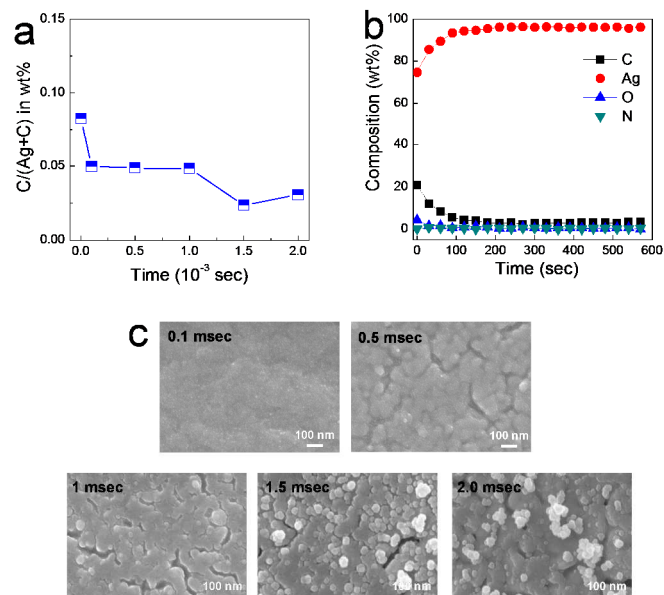


Figure 4. (a) Variation in  $C/(Ag+C)$  in weight ratio depending on photonic sintering times at  $3.0\text{ kV}$  and (b) composition profile data depending on an etching time for the Ag film photo-sintered at  $3.0\text{ kV}$  for  $1.0\text{ msec}$ , which were obtained from X-ray photoelectron spectroscopy analysis; the sputtering for etching gradually the surface layer was carried out at  $500\text{ eV}$ , and the data in Figure 4(a) was acquired after etching for  $390\text{ sec}$  at  $500\text{ eV}$ . (c) Top-view SEM images for Ag films photo-sintered at  $3.0\text{ kV}$  for different times ranging from  $0.1$  to  $2.0\text{ msec}$ . All of Ag films were formed on PI substrates.

tailor sophisticatedly capping molecular structures or to synthesize multi-functional organometallic precursors.

To clarify the chemical/microstructural evolution during the photo-annealing procedure, X-ray photoelectron spectroscopy (XPS) spectra were analyzed for Ag nanoparticle films photo-annealed at  $3.0\text{ kV}$  for different times ranging from  $0$  to  $2.0\text{ msec}$ , in conjunction with a scanning electron microscopy (SEM) based structural observation. Ag nanoparticle layers on PI substrates were studied for detail analysis, as the photon energy dependent evolution in Ag films did not evolve gradually on PET substrates due to the film peel-off at high energy dose conditions. The Ag  $3d$  spectra, seen in Figure S3, revealed that the pure silver phase did not undergo any chemical structural change, even following the incorporation of energetic photons during a prolonged time of  $2.0\text{ msec}$ . The weight ratio of  $C/(Ag+C)$ , calculated from XPS based composition analysis, suggested the capping molecules had been photo-chemically eliminated (Figure 4a). The uniformity of vertical composition along the film thickness was confirmed by depth-profile compositional data (Figure 4b). The weight ratio of  $C/(Ag+C)$  was measured to be  $0.083$  for an as-dried Ag nanoparticle film, and it decreased down to  $0.048$  and  $0.025$  after photo-annealing for  $0.1 - 1.0\text{ msec}$ , and  $1.5 - 2.0\text{ msec}$ , respectively. Based on the thermal analysis of Ag nanoparticles synthesized in this study, the weight fraction of capping molecules surrounding the nanoparticle surfaces was  $\sim 8\text{ wt\%}$  (Figure S4); taking the molecular structure of oleic acid into consideration, the weight ratio for the as-dried Ag film corresponds well to the thermal analysis data, which indicates the accuracy of the quantitative analysis of the residual carbon inside the Ag nanoparticle films. The absence of an N  $1s$  peak in the XPS spectra and the presence of carboxylate at a high binding energy in the C  $1s$  peak implies that the predominant

capping molecule comes from oleic acid, and not from octylamine (Figure S5).<sup>27</sup> The decrease of weight ratio, from 0.083 to 0.048, after a short 0.1 msec photon irradiation reflects the instant, partial decomposition of capping molecules by photo-chemical reaction with incident photons. The partial removal of the organic shell surrounding the metal nanoparticles is an important prerequisite for triggering microstructural densification that occurs by atomic migration between neighboring nanoparticles. As shown in Figure 4c, as the duration time increased from 0.1 to 1.0 msec, the microstructural transformation evolved with a relevant dependency on the dose of incident photons. For Ag nanoparticle films photo-annealed for 0.5 msec, small sub-grains, whose size was almost comparable to the diameter of Ag nanoparticles, were observed inside macroscopic large grains, indicative of a transient stage toward microstructural densification. The appropriate partial decomposition of capping molecules and the completion of microstructural densification explains how the low resistivity of  $8.0 \mu\Omega\cdot\text{cm}$  evolved as a result of the photo-annealing at 3.0 kV for 1.0 msec.

In addition, the presence of small amount of organic moieties, with a value of 0.05 for C/(Ag+C) weight ratio, enables the formation of highly conductive Ag films which adhere well onto plastic substrates, even after a general peeling-off test using adhesive tape, as shown in Figure S6. When the photo-annealing was applied for a duration time longer than 1.5 msec, the C/(Ag+C) weight ratio decreased further down to 0.025, and Ag layers partially peeled off from substrates right after a photo-annealing process. In thermal annealing-based approaches, the thermally annealed conductive Ag layers, composed of organic-free pure metallic phase, suffer from mechanical rupture off the underlying substrates, whereas as-dried Ag nanoparticle films adhere well to plastic substrates due to the anchoring capability of organic molecules through a secondary chemical interaction. In fact, in this study, the Ag nanoparticle films, sintered thermally at temperatures above  $250^\circ\text{C}$  for 1 hr, partially peeled off from substrates after adhesion tests, even showing the electrical resistivity below  $6 \mu\Omega\cdot\text{cm}$ . Organic adhesion promoters, which can remain even after thermal treatment at elevated temperatures, can be intentionally incorporated in colloidal solutions in order to improve the adhesion property; but the insulating organic phases in the metallic films also significantly degrade electrical conductivity.<sup>29</sup> Conventional thermal annealing techniques supply thermal energy for a prolonged time, generally longer than at least 10 min, which makes it difficult to precisely control the degree of organic moiety thermal decomposition. In contrast, as shown in Figure 4a, the time scale of instant photo-annealing methodology, at  $\sim 10^{-3}\text{sec}$ , controllably determines the remaining amount of decomposable organic capping molecules.

Figure 5a shows the flexibility test for conductive Ag layers on PET substrates under the bending radius down to 1 mm. The Ag layers were photo-annealed at 2.0 kV for 1.5 msec. The resistance did not vary when the bending radius decreased to 4 mm, and the resistance slightly increased under a bending radius below 2 mm. Note that the value of bending radius generally required for flexible devices is around 5 - 10 mm and a bending radius below 2 mm, almost accessible for foldable applications, is a harsh condition in flexibility tests. Most previous studies, which have reported wet nanoparticle-based metallic electrodes, did not obtain bending results under such harsh conditions.<sup>4</sup> This superior bendability is believed to result from the excellent adhesion of the fully converted film-like

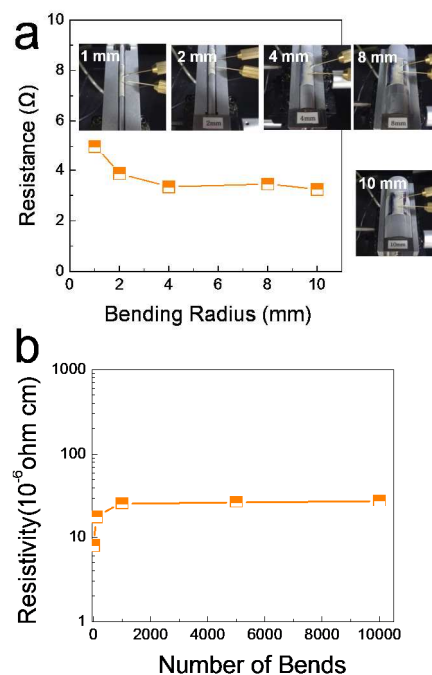


Figure 5. Resistance/resistivity variation of photo-sintered Ag films on PET substrate (a) as a function of bending radius ranging from 1 to 10 mm and (b) under the repeated bending test with a bending radius of 1.5 mm. The photo-sintering was carried out at 2.0 kV for 1.5 msec.

structure on PET substrates, obtained from the controlled interaction of photon energy with olate-terminated Ag nanoparticles. It is speculated that the slight increase of resistance under a bending radius below 2 mm results from the release of residual stress accumulated during a structural transformation for  $\sim\text{msec}$ . Figure 5b shows a repeated bending test conducted under an extremely harsh condition, 10,000 times with a bending radius of 1.5 mm; the motion picture of this bending test is provided as Video S1. After a slight increase during an initial stage due to the release of residual stress, the resistivity did not vary even up to 10,000 cycles, showing the relative resistivity change of 3.25. According to theoretical calculations,<sup>30</sup> the stably maintained resistivity of  $\sim 25 \mu\Omega\cdot\text{cm}$  during 10,000 cycles enables for the fabrication of mesh structured transparent conductive films with the transparency over 90 % and the sheet resistance lower than  $8 \Omega/\text{square}$ , for the cases with an invisible linewidth of  $8 \mu\text{m}$  and a pitch length of  $200 \mu\text{m}$ , and a linewidth of  $40 \mu\text{m}$  and a pitch length of  $900 \mu\text{m}$ . The linewidths of 8 and  $40 \mu\text{m}$  are the dimension of patterned structures achievable by representative nozzle-jet (electrohydrodynamic-jet)<sup>30</sup> and roll (gravure off-set) printing techniques.<sup>31</sup> As shown in Figure S7 and Video S2 (Supporting Information), a similar trend in electrical properties during the bending tests was confirmed for photo-annealed Ag layers on PI substrates, which implies that the resistance/resistivity variation observed in PET-based conductive Ag layers was not attributable to the photo-chemical degradation of PET substrates. To date, this successful demonstration in a harsh condition of highly flexible characteristics in Ag metal phase-driven conductive structures has not been reported even with Ag nanowires,<sup>32-34</sup> metal oxide/Ag nanowire hybrid structures,<sup>35</sup> laser annealed Ag nanoparticle assemblies,<sup>36,37</sup> structurally embedded Ag nanoparticles into polymeric matrix.<sup>31,38</sup> Figure S8 shows SEM images of the photo-annealed

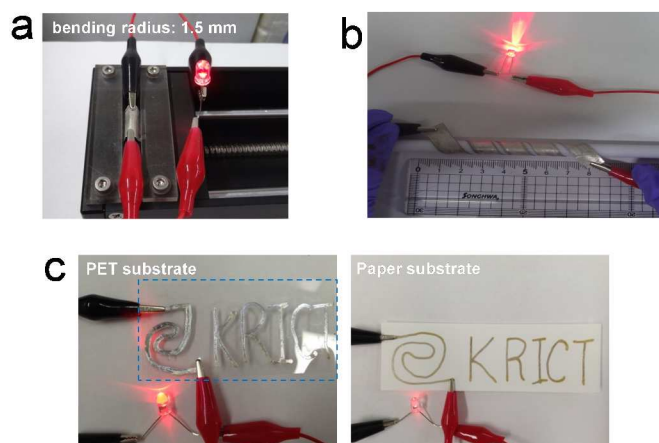


Figure 6. Photographs demonstrating (a) photo-sintered, fully flexible Ag electrode on PET substrate under a bending radius of 1.5 mm (b) fully rollable, large-area (20 cm in length) Ag electrode on PET substrate after a continuous photo-sintering process. (c) Photographs showing the pen-printed Ag electrodes on (c) PET and (d) paper substrate. The dashed line in (c) indicates the boundary of the transparent PET substrate. The photo-sintering was carried out at 2.0 kV for 1.5 msec and at 2.5 kV for 1.0 msec, for Ag films on PET and Paper substrate, respectively

Ag layers on PET substrates before/after the 10,000 cycle bending test under a radius of 1.5 mm. After this harsh bending test, the inter-grain displacement widened to some extent, which might be the origin of residual stress-related structural deformation and in turn, the slight degradation of electrical properties; but, the long-range film-like structure, observable in a low magnification SEM image, is still preserved, maintaining the electrically conductive pathways in the overall film.

Figure 6a is a simple demonstration showing that photo-annealed Ag layers on PET substrate are active, even when bent with a bending radius of 1.5 mm. Another processing advantage of the photo-annealing methodology is its facile application in large-area roll-to-roll fabrication. The wet chemical approach employing metallic nanoparticles can be utilized in simple coating or printing techniques, and is free from limitations for large area processability. The critical drawback in a roll-to-roll production of device-quality functional electrodes is the annealing step; conventional thermal annealing is not easily applicable to roll-to-roll processes, since a spatially long annealing zone is necessary to supply thermal energy for a prolonged time. In contrast, the very short duration of the pulsed instant photo-annealing allows for the facile fabrication of nanoparticle-derived conductive metallic layers on a moving stage. As shown in Figure 6b, a highly flexible Ag conductive layer was formed on a 20 cm-long PET substrate after photo-annealing for 60 sec. The UV-visible lamp used was 40 cm in length and 0.8 cm in width. The pulse on and off time was 1.5 and 1998.5 msec respectively, and the stage moving speed was 150 mm/min. The current investigation on continuous process in this study is a proof-of-concept, and it is expected that the production rate would be improved even further by additional synchronized optimization between the stage moving speed and the pulse on/off time. In addition to continuous process fabrication testing, the processing approach was tested for application in printing techniques by adopting a simple pen-printing system (Video S3). Among the various printing technologies, the pen printing technique is one of the more unique approaches for simply fabricating flexible devices.<sup>39</sup> As shown in Figure 7c, even after being combined with a shear

stress-involved pen printing process, the photo-annealed Ag layers exhibited resistivities of 8.7 and 15.2  $\mu\Omega\text{-cm}$  on PET and paper substrates, respectively. The slightly higher resistivity on the paper substrate resulted from the less dense packing of Ag nanoparticle assemblies on a rough substrate (Figure S9). The evaluation of other nozzle/stamp based printing techniques is underway based on the instant photonic sintering process for use with cost-effective PET and paper substrates.

#### 4. Conclusions

In summary, we demonstrated the highly conductive, flexible, rollable, printable features of olate passivated Ag nanoparticles on PI, PET, and paper substrates using the instant photonic sintering process. Without causing critical photo-chemical damages to the underlying substrates, the olate-Ag nanoparticle assemblies were converted to highly conductive bulk ones in a timescale of 1.0-1.5 msec at 2.0-3.0 kV, showing the electrical resistivity as low as 5.8-8.0  $\mu\Omega\text{-cm}$ . XPS based spectroscopy analysis, in conjunction with SEM observations of the photo-sintered Ag films, revealed that the instant supply of highly energetic photons made it possible to precisely control the degree of organic moiety thermal decomposition, enabling for the formation of suitably adhesive metallic films on polymeric substrates, as well as triggering a vigorous microstructural evolution. The photo-thermally derived conductive films showed extremely flexible properties during 10,000 times repeated bending tests even under a bending radius of 1.5 mm. In addition, the continuous process combined with a moving substrate stage demonstrated its practical application potential in a high throughput roll-to-roll process.

#### Acknowledgements

This research has been supported by the Korea Research Institute of Chemical Technology (KRICT), and partially received financial support from a National Research Foundation of Korea (NRF) grant funded by the Korea government (MSIP) (No. 2012R1A3A2026417).

#### Notes and references

<sup>a</sup> Division of Advanced Materials, Korea Research Institute of Chemical Technology (KRICT), Daejeon 305-600, Republic of Korea  
E-mail: youngmin@kRICT.re.kr; sjeong@kRICT.re.kr

<sup>b</sup> Department of Materials Science and Engineering, Yonsei University  
Seoul 120-749, Republic of Korea

Electronic Supplementary Information (ESI) available: the variation of photon energy and intensity as a function of voltage and duration time, the variation of substrate temperatures during a photonic sintering, Ag 3d XPS spectra for Ag films photo-sintered at 3.0 kV, TGA data of olate-Ag nanoparticles, O 1s and N 1s XPS spectra for Ag nanoparticles, the variation of resistance/resistivity for photo-sintered Ag films during repeated bending tests, SEM images for conductive Ag features on PET and paper substrates, and video files showing the bending tests and pen printing of olate-Ag nanoparticle ink. See DOI: 10.1039/b000000x/

- 1 Q. Cao, H. S. Kim, N. Pimparkar, J. P. Kulkarni, C. Wang, M. Shim, K. Roy, M. A. Alam, J. A. Rogers, *Nature*, 2008, **454**, 495.
- 2 M. Berggren, D. Nilsson, N. D. Robinson, *Nat. Mater.*, 2007, **6**, 3.
- 3 J. Perelaer, M. Klokkenburg, C. E. Hendriks, U. S. Schubert, *Adv. Mater.*, 2009, **21**, 4830.

- 4 A. Kamyshny, S. Magdassi, *Small*, 2014, DOI: 10.1002/smll.201303000
- 5 M. Hoesel, F. C. Krebs, *J. Mater. Chem.*, 2012, **22**, 15683.
- 6 Y. Galagan, E. W. C. Coenen, R. Abbel, T. J. V. Lammeren, S. Sabik, M. Barink, E. R. Meinders, R. Andriessen, P. W. M. Blom, *Org. Electron.*, 2013, **14**, 38.
- 7 J. S. Kang, J. Ryu, H. S. Kim, H. T. Hahn, *J. Electron. Mater.*, 2011, **40**, 2268.
- 8 W.-H. Chung, H.-J. Hwang, S. -H. Lee, H.-S. Kim, *Nanotechnology*, 2013, **24**, 35202.
- 9 H.-J. Hwang, W.-H. Chung, H. -S. Kim, *Nanotechnology*, 2012, **23**, 485205.
- 10 R. Abbel, T. V. Lammeren, R. Hendriks, J. Ploegmakers, E. J. Rubingh, E. R. Meinders, W. A. Groen, *MRS Comm.*, 2012, **2**, 145.
- 11 D. Kim, S. Jeong, H. Shin, Y. Xia, J. Moon, *Adv. Mater.*, 2008, **20**, 3084.
- 12 S. Jeong, H. C. Song, W. W. Lee, Y. Choi, S. S. Lee, B.-H. Ryu, *J. Phys. Chem. C*, 2010, **114**, 22277.
- 13 S. Jeong, H. C. Song, W. W. Lee, H. J. Suk, S. S. Lee, T. Ahn, J. W. Ka, Y. Choi, B.-H. Ryu, *J. Mater. Chem.*, 2011, **21**, 10619.
- 14 S. Jeong, H. C. Song, W. W. Lee, Y. Choi, B.-H. Ryu, *J. Appl. Phys.*, 2010, **108**, 102805.
- 15 J. Perelaer, P. J. Smith, D. Mager, D. Soltman, S. K. Volkman, V. Subramanian, J. G. Korvink, U. S. Schubert, *J. Mater. Chem.*, 2010, **20**, 8446.
- 16 S. Wunscher, S. Stumpf, A. Teichler, O. Pabst, J. Perelaer, E. Beckett, U. S. Schubert, *J. Mater. Chem.*, 2012, **22**, 24569.
- 17 I. Reinhold, C. E. Hendriks, R. Eckardt, J. M. Kranenburg, J. Perelaer, R. R. Baumann, U. S. Schubert, *J. Mater. Chem.*, 2009, **19**, 3384.
- 18 S. Wunscher, S. Stumpf, J. Perelaer, U. S. Schubert, *J. Mater. Chem. C*, 2014, **2**, 1642.
- 19 S. H. Ko, H. Pan, C. P. Grigoropoulos, C. K. Luscombe, J. M. J. Frechet, D. Poulidakos, *Appl. Phys. Lett.*, 2007, **90**, 141103
- 20 J. Perelaer, M. Klokkenburg, C. E. Hendriks, U. S. Schubert, *Adv. Mater.*, 2009, **21**, 4830.
- 21 J. Perelaer, R. Jani, M. Grouchko, A. Kamyshny, S. Magdassi, U. S. Schubert, *Adv. Mater.*, 2012, **24**, 3993.
- 22 M. Grouchko, A. Kamyshny, C. F. Mihailescu, D. F. Anghel, S. Magdassi, *ACS Nano*, 2011, **5**, 3354.
- 23 M. Layani, M. Grouchko, S. Shemesh, S. Magdassi, *J. Mater. Chem.*, 2012, **22**, 14349.
- 24 M. Layani, S. Magdassi, *J. Mater. Chem.*, 2011, **21**, 15378.
- 25 B.-Y. Wang, T.-H. Yoo, Y. -W. Song, D.-S. Lim, Y.-J. Oh, *ACS Appl. Mater. Interfaces*, 2013, **5**, 4113.
- 26 W.-S. Han, J.-M. Hong, H.-S. Kim, Y.-W. Song, *Nanotechnology*, 2011, **22**, 395705.
- 27 S. Jeong, S. H. Lee, Y. Jo, S. S. Lee, Y. H. Seo, B. W. Ahn, G. Kim, G.-E. Jang, J.-U. Park, B.-H. Ryu, Y. Choi, *J. Mater. Chem. C*, 2013, **1**, 2704.
- 28 T.-H. Yoo, S.-J. Kwon, H.-S. Kim, J.-M. Hong, J. A. Lim, Y.-W. Song, *RSC Adv.*, 2014, **4**, 19375.
- 29 D. Jang, D. Kim, B. Lee, S. Kim, M. Kang, D. Min, J. Moon, *Adv. Funct. Mater.*, 2008, **18**, 2862.
- 30 Y. Jang, J. Kim, D. Byun, *J. Phys. D: Appl. Phys.*, 2013, **46**, 155103.
- 31 S. Jung, S. Lee, M. Song, D.-G. Kim, D. S. You, J.-K. Kim, C. S. Kim, T.-M. Kim, K.-H. Kim, J.-J. Kim, J.-W. Kang, *Adv. Energy Mater.*, 2014, **4**, 1300474.
- 32 J. Lee, P. Lee, H. B. Lee, S. Hong, I. Lee, J. Yeo, S. S. Lee, T.-S. Lee, D. Lee, S. H. Ko, *Adv. Funct. Mater.*, 2013, **23**, 4171.
- 33 S. De, T. M. Higgins, P. E. Lyons, E. M. Doherty, P. N. Nirmalraj, W. J. Blau, J. J. Boland, J. N. Coleman, *ACS Nano*, 2009, **3**, 1767.
- 34 D. Langley, G. Giusti, C. Mayousse, C. Celle, D. Bellet, J.-P. Simonato, *Nanotechnology*, 2013, **24**, 452001.
- 35 A. Kim, Y. Won, K. Woo, C.-H. Kim, J. Moon, *ACS Nano*, 2013, **7**, 1081.
- 36 J. Yeo, G. Kim, S. Hong, M. S. Kim, D. Kim, J. Lee, H. B. Lee, J. Kwon, Y. D. Shin, H. W. Kang, H. J. Sung, J.-H. Choi, W.-H. Hong, J. M. Ko, S.-H. Lee, S.-H. Choa, S. H. Ko, *J. Power Sources*, 2014, **246**, 562.
- 37 S. Hong, J. Yeo, G. Kim, D. Kim, H. Lee, J. Kwon, H. Lee, P. Lee, S. H. Ko, *ACS Nano*, 2013, **7**, 5024.
- 38 A. Mahajan, L. F. Francis, C. D. Frisbie, *ACS Appl. Mater. Interfaces*, 2014, **6**, 1306.
- 39 A. Russo, B. Y. Ahn, J. J. Adams, E. B. Duoss, J. T. Bernhard, J. A. Lewis, *Adv. Mater.*, 2011, **23**, 3426.

## Graphical Abstract

Highly Flexible, Rollable, Printable Ag Conductive Features are generated on PET and paper substrates through instant continuous photonic sintering for olate-terminated Ag nanoparticles.

